Soft Matter

Cite this: *Soft Matter*, 2012, **8**, 11163

www.rsc.org/softmatter

PAPER

Successive order–order transitions of the hierarchical morphology of a dendron-jacketed block copolymer *via* subsequent stretching alignment and self-assembly†

Wei-Tsung Chuang,* Yen-Chih Huang, Chun-Jen Su, U.-Ser Jeng* and Hwo-Shuenn Sheu

Received 8th June 2012, Accepted 17th August 2012
DOI: 10.1039/c2sm26331a

A dendron amphiphile 4′-(3,4,5-trioctyloxybenzoyloxy)benzoic acid (TOB) is designated to bind, *via* hydrogen bonding, into vinylpyridine blocks of polystyrene-*block*-poly(4-vinylpyridine) (PS-*b*-P4VP), for a high TOB grafting density of 0.7. Stretching followed by specific annealing enables the TOB-jacketed P4VP blocks, P4VP(TOB)$_{0.7}$, to exhibit several liquid crystal (LC) phases with increasingly better packing strength, from bilayer smectic to a highly oriented and hexagonally packed columnar phase; thereby, the global structure of the supramolecular complex PS-*b*-P4VP(TOB)$_{0.7}$ evolves from body-centered-cubic to face-centered-cubic (FCC), then to a highly oriented tetragonally perforated layer (TPL) structure, as evidenced by *in situ* small- and wide-angle X-ray scattering and transmission electron microscopic images. In particular, captured is the subtle transition of the FCC-packed PS domains, *via* an epitaxial extension along the ⟨110⟩ direction, into the perforated layers of TPL. Modulation of the local and global packing sequence *via* external stretching and annealing proves to be an efficient way in preparing oriented and hierarchically ordered dendron-jacketed block copolymers.

1. Introduction

Morphology control at the nanometer scale has enabled many exciting materials with tailored functions. One of the developments is to attach amphiphilic molecules *via* noncovalent interactions to block copolymers (BCPs) for side-chain functionalized supramolecules;[1–12] this has quickly drawn considerable attention due to synthetic simplicity and tunable hierarchical structures. Such a type of supramolecular complex features in versatile liquid crystal (LC) phases, having characteristic lengths of several nanometers, nested in globally ordered BCP domains of lattice constants of several tens to hundreds of nanometers. Recently, several dendrons designed for strong self-affinity were jacketed into BCPs; these dendrons could override the BCP phase separations and actively form a locally layered or columnar LC phase.[1–6] For instance, Mezzenga and co-workers[2,6] reported that cationic dendronized BCPs incorporated with anionic surfactants *via* supramolecular interactions could self-organize into several different LC phases including rectangularly, tetragonally and hexagonally packed columns within lamellar microdomains of the BCPs for hierarchically ordered structures. Also reported were the dendron–coil type of supramolecular systems[13] for comparable global and local supramolecular interactions, leading to very complicated elf-assembly morphologies.

Previously, we reported that dendron 4′-(3,4,5-trioctyloxybenzoyloxy)benzoic acid (TOB) could selectively incorporate, *via* hydrogen binding, into the P4VP blocks of poly(styrene)$_{192}$-*block*-poly(4-vinylpyridine)$_{181}$ (PS-*b*-P4VP).[3] TOB was included in the Percec-type hybrid dendron family as (3,4,5-4)8G1-COOH.[1] With modulated TOB grafting density, the supramolecular complex was shown to exhibit distinctly different microphase separation behaviors similar to that for coil–coil,[14] comb–coil,[6–9] or rod–coil BCPs,[15–17] resulting in rich hierarchically ordered structures. Especially, at the highest TOB grafting density of 0.7 hexagonally packed columnar LC domains (HEX$_{col}$) of P4VP(TOB)$_{0.7}$ could form and direct the microphase separation of the BCP host for tetragonally perforated layers (TPL).[3] The formation mechanism of such a HEX$_{col}$-*within*-TPL structure, however, is not fully understood. Unveiling the trapping mechanism of this rarely observed hierarchical structure would help to establish guidelines for preparing hierarchically ordered morphologies of dendron-jacketed BCPs.

Using *in situ* small- and wide-angle X-ray scattering (SAXS and WAXS), in addition to transmission electron microscopy (TEM) and differential scanning calorimetry (DSC), we elucidate here that external stretching followed by annealing leads to several LC phases of P4VP(TOB)$_{0.7}$ complex with increasingly better packing order; transitions of the LC phases furthermore drive the hierarchical morphology of PS-*b*-P4VP(TOB)$_{0.7}$ for successive order–order transitions to the final HEX$_{col}$-*within*-TPL.

National Synchrotron Radiation Research Center, 101 Hsin-Ann Road, Hsinchu 30076, Taiwan. E-mail: weitsung@nsrrc.org.tw; usjeng@nsrrc.org.tw; Fax: +886-3-578-3813; Tel: +886-3-578-0281 ext. 7125

† Electronic supplementary information (ESI) available: WAXS profiles, 2D GISAXS patterns, FI-IR spectra and TEM images. See DOI: 10.1039/c2sm26331a

2. Experimental section

2.1 Materials

TOB dendron, 4′-(3,4,5-trioctyloxybenzoyloxy)benzoic acid (Scheme 1) was prepared following the modified procedures reported previously.[3] Diblock copolymer PS_{192}-*b*-$P4VP_{181}$, with respective weight-average block molecular masses of 20 and 19 kDa and a polydispersity index of 1.09, was received from the Polymer Source Inc. Blend films of PS-*b*-P4VP(TOB)$_x$ were cast from chloroform solutions containing 1 wt% mixture of the copolymer and TOB, for $x = 0.7$. The corresponding volume fractions of the PS phase (ϕ_{PS}) = 0.19 was deduced based on the densities of PS (1.047 g cm^{-3}), P4VP (1.114 g cm^{-3}) and TOB (1.112 g cm^{-3}, determined by automatic gas displacement pycnometer) at room temperature; ϕ_{PS} changes less than 1% in the studied temperature range (20–180 °C) according to the density changes of PS and P4VP reported previously.[18]

2.2 Methods

The sample thin films (*ca.* 0.5 mm in thickness) were slowly dried under a controlled solvent vapor pressure at ambient temperature. Subsequently, the films were stretched at 120 °C for a drawing ratio of *ca.* 2, followed by 85 °C annealing with tension released for 6–12 h. A similar sample, but without stretching treatment, was heated from 25 to 180 °C then cooled back, during which *in situ* X-ray scattering measurements were made. Small- and wide-angle X-ray scattering (SAXS and WAXS) measurements were performed respectively at the BL23A SWAXS endstation[19] and BL01C2 XRD endstation of the National Synchrotron Radiation Research Center (NSRRC), Taiwan, with an X-ray wavelength λ of 1.55 Å or 1.03 Å. All SAXS data collected with a MarCCD165 area detector were rigorously corrected for electronic noise, sample transmission, background scattering and detector sensitivity, and calibrated by polyethylene for the absolute intensity of SAXS and silver behenate for the scattering wavevector q (defined by $4\pi\lambda^{-1}\sin\theta$ with the scattering angle 2θ).[19] One-dimensional (1D) SAXS profiles were circularly averaged from the corresponding 2D scattering patterns. WAXS data collected with a Mar345 image plate were placed on the q-axis calibrated by the diffractions from mixed powders of silicon and silver behenate. For oriented structures, SAXS and WAXS patterns were respectively taken with three mutually orthogonal beam incidences with respect to the sample orientations.

Glass transition temperatures (T_g) of the samples were observed using a Perkin-Elmer Diamond differential scanning calorimeter (DSC), with temperature and heat flow calibrated using standard materials of indium and zinc under the same sample environment. All DSC measurements were performed with a heating rate of 10 °C min^{-1}, under dry nitrogen flow. The real space images of PS-*b*-P4VP(TOB)$_{0.7}$ were observed by a Philips Tecnai G^2 F20 TEM at 120 kV. TEM samples were cryo-sectioned at −60 °C using a Leica Reichert Ultracut-E-ultramicrotome; sections of 30–70 nm thickness were collected on 400-mech gold grids and stained by iodine vapor for *ca.* 30–70 min. TEM images were taken with different sample orientations for 3D structural information.

3. Results and discussion

To kinetically trap the TPL structure of the supramolecular complex PS-*b*-P4VP(TOB)$_{0.7}$, we have designated a special process to modulate the relative strengths of the two interacting phase separations of the copolymer and the dendron-jacketed sub-domains of P4VP(TOB)$_{0.7}$ in different length scales.[12] For this, the T_g values of the P4VP(TOB)$_{0.7}$ and PS blocks revealed from the DSC traces (as shown in Fig. 1) for the PS-*b*-P4VP(TOB)$_{0.7}$ film provide a critical reference in selecting parameters for the structural trapping process, which involves (i) heating the sample above both the T_g values of PS (~110 °C) and P4VP(TOB)$_{0.7}$ (~50 °C) domains, (ii) followed by an appropriate thermal stretching to facilitate alignment of the jacketed TOB

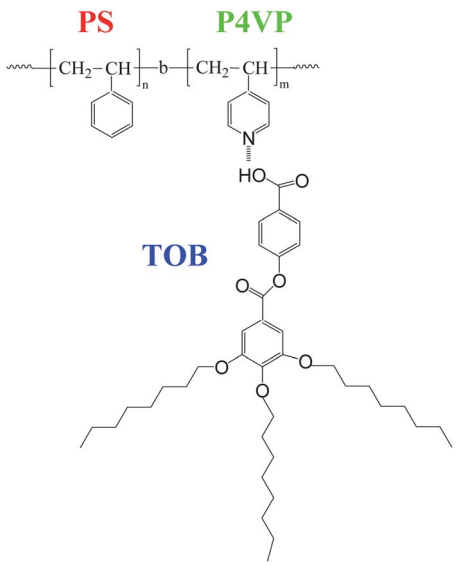

Scheme 1 A schematic illustration of the supramolecular complex of PS-*b*-P4VP and TOB *via* hydrogen bonding.

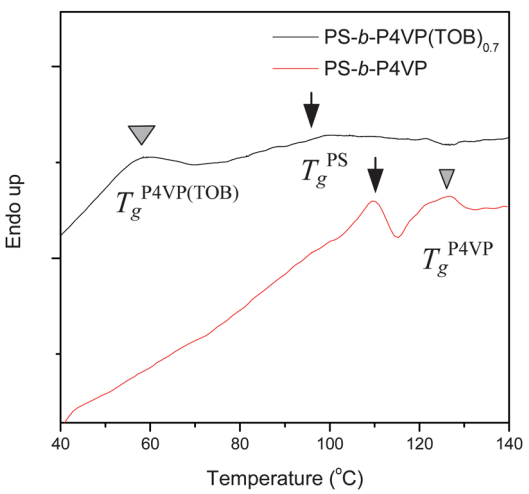

Fig. 1 DSC traces for PS-*b*-P4VP(TOB)$_{0.7}$ and neat PS-*b*-P4VP. The large and small triangles respectively indicate the T_g values of the P4VP(TOB)$_{0.7}$ complex and neat P4VP blocks, whereas the arrows indicate the T_g of PS blocks.

along the softened and stretched P4VP chains, then (iii) annealing at 85 °C just below the T_g of PS, but above the T_g of P4VP(TOB)$_{0.7}$, with the stress released. We note that TOB could disperse well and bind to pyridine of P4VP to form LC phases in the supramolecular complex, on the basis of the X-ray diffraction result (Fig. S1, ESI†) revealing no observable TOB crystalline domains.

3.1 Stretching-facilitated TPL structure

Shown in Fig. 2 are the representative 2D SAXS patterns taken *in situ* (with beam incidence along the *Y* direction as indicated) for a PS-*b*-P4VP(TOB)$_{0.7}$ film in the designated stretching and annealing process. The SAXS pattern for the as-cast film (Fig. 2a) exhibits powder rings, with the scattering peak positions corresponding to a body-centered-cubic (BCC) structure; the lattice extracted from the first reflection is 44 nm. In Fig. 2b, the powder rings (01) and (02) at $q = 1.48$ and 2.96 nm^{-1} (corresponding to a lamellar spacing $d = 4.2$ nm) reveal randomly oriented bilayer smectic (Sm) domains of P4VP(TOB)$_{0.7}$, presumably embedded in the BCC structure. FT-IR result (Fig. S2, ESI†) indicates that the LC packing is mainly facilitated by the hydrogen bonding of TOB with the pyridines groups of the P4VP blocks of the copolymer (*cf.* Scheme 1).[3]

When the sample was subjected to stretching at 120 °C for a stretching ratio of ~2, the symmetric scattering pattern of BCC (Fig. 2a) transformed into an asymmetrical one, with six strip-like reflections (Fig. 2c) resembling that for a distorted FCC structure. Although the scattering pattern might be reminiscent of a chevron structure of wavy layers,[20] the indexed (200) and (111) FCC reflections differ substantially in the q_z positions; which would correspond to large layer undulations amounting to roughly 20 nm (estimated from the peak positions) out of the layer planes for a chevron structure. This would be unfavourable due to a high conformation energy cost, as compared to the proposed FCC structure of deformed PS domains transited from the BCC spherical domains (illustrated further below). Furthermore, the periodic reflections (arc shape) in Fig. 2d (corresponding to *d*-spacing = 4.2 nm) are emphasized in the equatorial direction, indicating formation of a highly oriented Sm phase with the layer normal perpendicular to the stretching direction (*Z*). In addition, the 2D WAXS image in the inset of Fig. 2d exhibits a powder ring with an emphasis on the meridian direction. This may be contributed by a stretching-enabled rotation alignment of the TOB fan-like molecular plans (comprising the coplanar mesogen and three aliphatic chains), having a π–π stacking along the stretching direction (or perpendicular to the Sm layer stacking) and the hence concentrated aliphatic chains of a liquid-like ordering (*cf.* the cartoon in the inset of Fig. 2d).

With the sample annealing temperature lowered to 85 °C, anisotropic contraction of the sample film along mainly the stretching direction allowed P4VP chains to recoil for greatly enhanced packing of TOB. During the subsequent annealing, the six-strip FCC pattern in Fig. 2c gradually sharpened (Fig. S3, ESI†) and transformed into strong periodic reflections of a layer-like structure along the meridian direction, accompanied by weaker off-meridian reflections (Fig. 2e). These changes reveal a transformation from the FCC structure to perforated layers. The

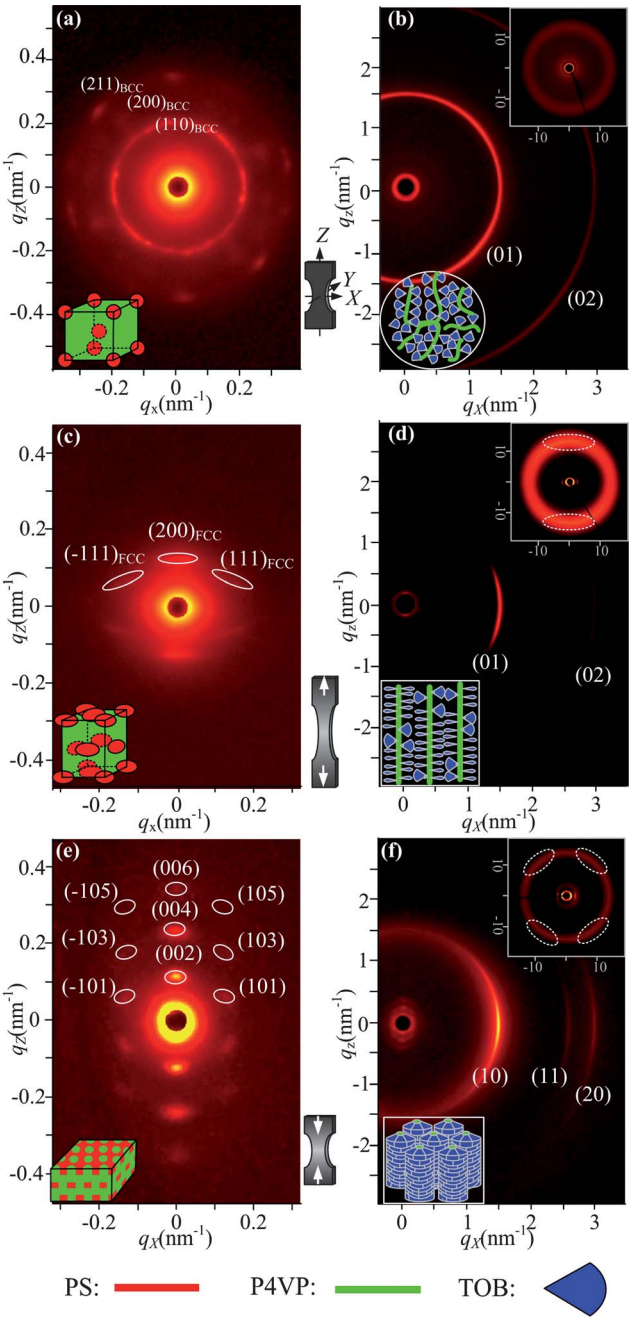

Fig. 2 *In situ* 2D SAXS patterns covering two different *q*-ranges for a PS-*b*-P4VP(TOB)$_{0.7}$ film subjected to subsequent stretching and annealing: from the as-cast film, (a) and (b), to ~two-fold stretching at 120 °C, (c) and (d), followed by stress releasing and 6 h annealing at 85 °C, (e) and (f). Reflections in the low-*q* region are indexed according to BCC (a), distorted FCC (c) and TPL structures (e). Reflections in the high-*q* region are indexed according to Sm (b) and (d) and HEX$_{col}$ (f) LC phases. Also shown in the insets of (b), (d) and (e) are the corresponding 2D WAXS patterns, with circled zones indicating the orientations of TOB stacking. The film stretching direction is along *Z* (or q_z), as indicated. PS, P4VP and TOB domains are respectively coded in red, green and blue.

reflections could be indexed rather well using a body-centered tetragonal (*I*4/*mmm* space group) lattice with alternative A–B layer stacking of P4VP(TOB)$_{0.7}$ columnar layers and P4VP(TOB)$_{0.7}$-perforated PS layers. From the reflection

positions, two in-plane lattice parameters $a = b = 47.4$ nm are extracted for the perforated structure and an across-plane lattice parameter $c = 102.6$ nm for layer stacking. Exhibited in Fig. 2f is the corresponding HEX scattering pattern of highly oriented columns (HEX_{col}) of P4VP(TOB)$_{0.7}$, revealing a local LC phase transformation from the oriented Sm layers into HEX_{col}. From the first peak position at $q_{10} = 1.51$ nm^{-1}, we can extract a lattice parameter a_{col} of 4.8 nm and a tighter column center-to-center distance of 4.16 nm. Such a transformation originates from the key enhancement of the TOB packing, as revealed from the changing of 2D WAXS pattern to the four-lobe scattering (the inset of Fig. 2f); this pattern suggests that the stretching-aligned, fan-like molecular plans are densely stacked and oriented into rigid LC columns upon the shrinking of P4VP chains. In view of the inclined angle of 55° deduced from the four-lobe positions (*cf.* Fig. S4, ESI†), the TOB molecular fans likely spiral down along the P4VP chains in forming the rigid LC columns for an optimum spacing filling efficiency (*cf.* inset of Fig. 2f). The structural features of the HEX_{col}-*within*-TPL of PS-*b*-P4VP(TOB)$_{0.7}$ *in situ* observed are, in general, consistent with that shown in our previous report with a pre-processed sample;[3] the structural evolution observed here, however, unveils the critical local-prior-to-global ordering sequence for trapping the TPL structure.

When the *in situ* processed sample was cooled down to ambient temperature, the HEX_{col}-*within*-TPL structure could be maintained well; the structure could persist with reasonable thermal stability up to reheating to ~90 °C (Fig. 3), before the T_g of PS. This behavior is consistent, in general, with many previous theoretical and experimental studies, showing that coil–coil BCPs could at best form metastable perforated layer structures, with the minor component typically occupying a volume fraction of 0.3–0.4.[14] Nevertheless, the TPL structure of the supramolecular complex PS-*b*-P4VP(TOB)$_{0.7}$ could exist with a lower volume fraction of PS ($\phi_{PS} = 0.19$); this presumably was owing to the especially rigid HEX_{col} phase of P4VP(TOB)$_{0.7}$ (of high grafting density), having a strong segregation for planar inter-material dividing surfaces (IMDS).

3.2 FCC-to-TPL phase transformation route

Cartoons in Fig. 4 illustrate a proposed transformation route of the PS-*b*-P4VP(TOB)$_{0.7}$ from Sm-*within*-BCC to the highly oriented HEX_{col}-*within*-TPL morphology *via* Sm-*within*-FCC structure. Specifically, under the high stretching ratio of *ca.* two-fold at 120 °C, the P4VP(TOB)$_{0.7}$ domains should be highly deformed and aligned along the stretching direction. This would force spherical PS domains in the BCC structure to flatten for larger IMDS perpendicular to the stretching, thereby accommodate the aligned LC (Sm) domains of P4VP(TOB)$_{0.7}$ for an FCC structure. Extension of the PS domains along the stretching would be very difficult, as the IMDS is now strongly confined (or trapped) by the highly oriented LC domains preferring planar IMDS. Upon releasing of the stress, the deformed PS domains would flatten furthermore to response to the lateral expansion of the P4VP(TOB)$_{0.7}$ domains for columnar packing, owing to recoiled P4VP chains (or the film) along the stretching direction. As a result, the overstretched FCC PS domains could interconnect and transform into perforated PS layers for the TPL structure.

On this basis of the FCC (111) reflection (Fig. 2c), a lattice of $a \sim 67 \pm 3$ nm is extracted for the intermediate structure observed prior to TPL. Simple geometrical deduction shows a shortest inter-spacing of the PS domains $a/\sqrt{2} = 47$ nm along the ⟨110⟩ direction (Fig. 4). When the lateral dimension is stretched over this size, the PS domains can interconnect into a perforated layer along the FCC ⟨110⟩ direction. Consequently, the previous P4VP(TOB)$_{0.7}$ matrix blocks are now squeezed into perforating

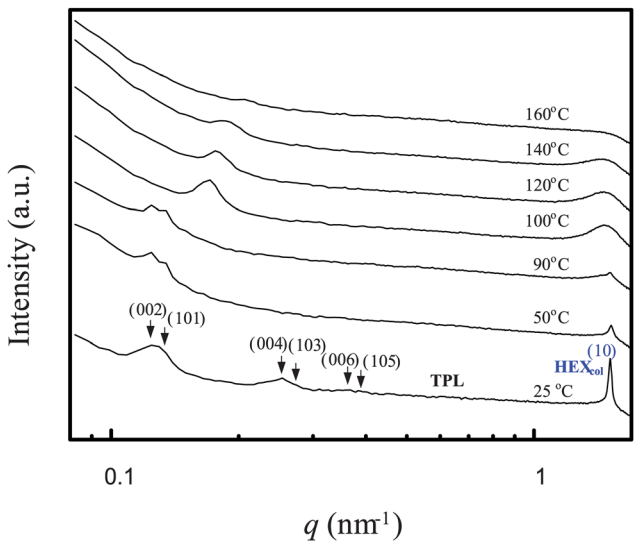

Fig. 3 SAXS profiles collected over a heating process for a PS-*b*-P4VP(TOB)$_{0.7}$ film with an initial structure of HEX_{col}-*within*-TPL. Note that for the 25 °C case the reflection peaks are broadened significantly in the circularly averaged SAXS profile (*cf.* the spot-like reflections in Fig. 1f).

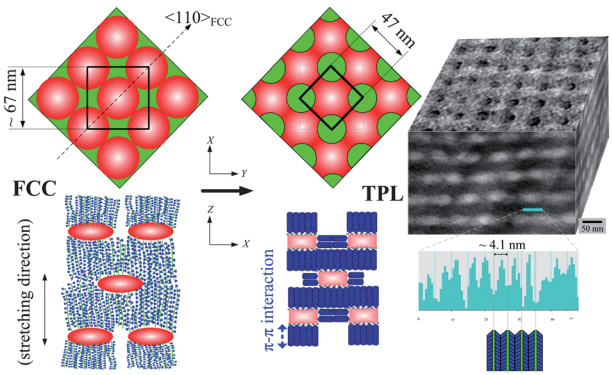

Fig. 4 Cartoons in the top row showing the proposed FCC-to-TPL structural transition of PS-*b*-P4VP(TOB)$_{0.7}$: the spherical PS domains (in red) stretch along the FCC ⟨110⟩ direction into PS matrix layers perforated with P4VP(TOB)$_{0.7}$ domains. The cartoons in the bottom row illustrate the side views of the structural transformation. Also shown is a 3D representation of the TPL structure constructed from the orthogonal TEM images. Dark zones are for iodine-stained P4VP blocks. The thick bar on the TEM images marks the location where the sectioned electron density profile (shown below the TEM images) is taken; the alternate low and high densities correspond to the P4VP-cores and TOB-shells as indicated by the cartoon below.

domains, with the inter-domain spacing of $a/\sqrt{2} = 47$ nm (Fig. 4) coinciding exactly with the lattice parameter a of the observed TPL structure (Fig. 2c). This seamless match in the transformation of the lattice size of the FCC to that of the TPL strongly supports the FCC-to-TPL transition route proposed. Correspondingly, the TEM images in Fig. 4 evidence the final TPL structure of PS-*b*-P4VP(TOB)$_{0.7}$ and the significantly flattened and interconnected PS (perforated layer) domains, of dimensions of ~50 nm in width and 20 nm in thickness (further details are shown in Fig. S5, ESI†). The P4VP chains confined in the core of the P4VP(TOB)$_{0.7}$ columns have a lateral dimension of *ca.* 0.6 nm, as estimated from the difference between the columnar core–core distance (4.1 nm) and the columnar shell thickness (estimated from two times of the 55°-projected TOB size onto the columnar plane ~1.7 nm). Such columnar core size may correspond to a confined single P4VP chain of disordered helical conformation, as suggested previously by Percec *et al.* for dendron-jacketed polymers;[21] the helical conformation may associate with the previously proposed spiral down structure of TOB in forming rigid P4VP(TOB)$_{0.7}$ LC columns.

3.3 Thermodynamically favored FCC phase

To illustrate the importance of the pre-aligned LC phase *via* external stretching in the formation of TPL structure with PS-*b*-P4VP(TOB)$_{0.7}$, we have also conducted *in situ* SAXS for a similar sample subject to a heating treatment, but without stretching. Illustrated in Fig. 5a and b are a series of SAXS profiles (covering two different q-ranges) circularly averaged from the corresponding 2D powder-ring patterns obtained for the PS-*b*-P4VP(TOB)$_{0.7}$ complex in a heating–cooling process between 25–180 °C. For the as-cast film at 25 °C, the SAXS profile reveals a hierarchically ordered morphology of Sm-*within*-BCC, similar to that shown in Fig. 2a. When the sample temperature was elevated to 60–80 °C for softened P4VP(TOB)$_{0.7}$, SAXS peaks in the higher-q region were slightly shifted and enhanced (Fig. 5b) for a peak position ratio of $1 : 3^{1/2} : 2$, revealing a LC phase transition from the Sm phase to loosely 2D-hexagonally-packed columnar domains. Meanwhile, the SAXS peaks in the lower-q region (Fig. 5a) for the BCC structure were significantly deteriorated, presumably, by the dominant LC ordering process.

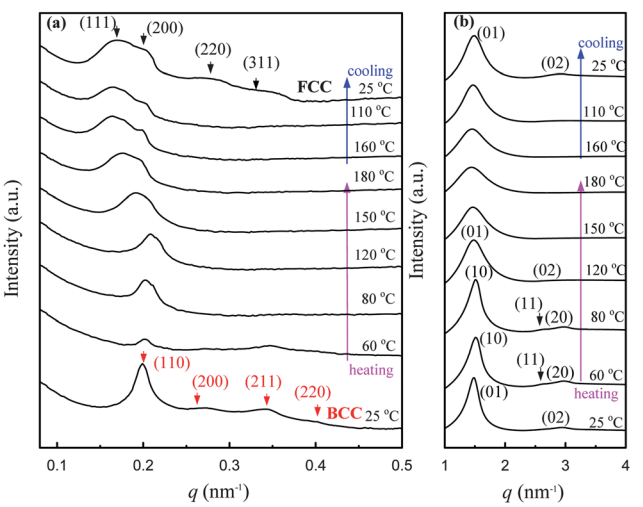

Fig. 5 Temperature-dependent SAXS profiles for an as-cast film of PS-*b*-P4VP(TOB)$_{0.7}$. (a) In the lower-q region, the reflections are indexed according to BCC and FCC structures for the globally ordered morphology. (b) In the higher-q region for the corresponding local ordering, the reflections are indexed with either Sm phase or HEX$_{col}$ phase characterized by (11) reflection.

At 120 °C, the largely deteriorated peaks in Fig. 5b indicate a relaxation of the local packing to Sm; at 150 °C and above, a single halo reveals further degradation of the LC packing to a nematic phase owing to diminished hydrogen bonding at high temperatures. Closely correlated were the successively enhanced and shifted SAXS peaks in the lower-q region (Fig. 5a), implying improvement on the ordering of global morphology upon relaxation of the local LC packing of P4VP(TOB)$_{0.7}$. At 180 °C, embryo (111) and (200) peaks of an FCC structure appeared (Fig. 5a) and developed into characteristic peaks of a position ratio of $1 : (4/3)^{1/2} : (8/3)^{1/2} : (11/3)^{1/2}$ after the sample cooled down to room temperature. The thermally stable FCC structure has a lattice parameter 67 nm deduced from the (111) reflection. Concomitantly improved lamellar peaks in the higher-q region (Fig. 5b) suggest locally and passively formed Sm domains of P4VP(TOB)$_{0.7}$ nested in the FCC morphology.

Overall, the structural evolution observed in the heating–cooling process indicates that without pre-stretching alignment the local LC packing takes only a passive role in the self-assembly of the supramolecular complex, leading to the hierarchical structure of Sm-*within*-FCC. Moreover, the result suggests that the solvent-induced TOB packing for the BCC phase would dissipate in the thermal treatment for a thermodynamically favored FCC structure. This BCC-to-FCC structural transformation might be resulted from diminished hydrogen-bonding and more active amphiphilic nature of TOB at high temperatures. Consequently, TOB molecules released from the P4VP(TOB)$_{0.7}$ phase might relocate near the vertexes of the Wigner–Seitz cells, thereby alleviating the stretching constraint (the conformational energy) of the P4VP chains (coronal blocks) in the FCC lattice.[22–24] A similar BCC-to-FCC phase transformation was also observed in sphere-forming BCP/homopolymer (A-*b*-B/h-A) blends.[24]

4. Conclusions

We have shown that *via* successive order–order transitions a hierarchical morphology of HEX$_{col}$-*within*-TPL can be kinetically trapped for the supramolecular complex PS-*b*-P4VP(TOB)$_{0.7}$. This is enabled *via* manipulation of the packing sequence of the dendron-jacketed P4VP(TOB)$_{0.7}$ complexes (*via* TOB packing) and the host BCPs in different length scales. With the critically enhanced TOB packing *via* external stretching alignment, the rigid P4VP(TOB)$_{0.7}$ columns can pack actively for highly oriented and ordered mesomorphic HEX$_{col}$ domains of planar IMDS. Consequently, the host copolymer complex self-assembles like rod–coil BCPs for the TPL structure.[15,16] We emphasize that the designated route for the TPL trapping relies critically on the subsequent local and global packing, modulated *via* stretching and annealing. An underlying prerequisite of the structure trapping process is the high dendron grafting density, allowing a sufficient LC packing strength of the dendron-jacketed copolymer blocks for rigid HEX$_{col}$ domains. Note that the

high dendron packing density depends largely on the designated molecular architecture of TOB, having balanced aliphatic chains and mesogenic group for a good dispersion in the copolymer blocks.

Acknowledgements

We thank Ms K.-F. Liao and Mr W.-B. Su for the help in SAXS measurements. Financial support from the National Science Council (grant numbers: NSC 99-2218-E-213-001-MY3 and NSC 99-2112-M 213-002-MY3) is gratefully acknowledged.

Notes and references

1 B. M. Rosen, C. J. Wilson, D. A. Wilson, M. Peterca, M. R. Imam and V. Percec, *Chem. Rev.*, 2009, **109**, 6275.
2 C. Li, A. D. Schlüter, A. Zhang and R. Mezzenga, *Adv. Mater.*, 2008, **20**, 4530.
3 W. T. Chuang, H. S. Sheu, U. Jeng, H. H. Wu, P. D. Hong and J. J. Lee, *Chem. Mater.*, 2009, **21**, 975.
4 K. Albrecht, A. Mourran, X. Zhu, T. Markkula, J. Groll, U. Beginn, W. H. de Jeu and M. Moeller, *Macromolecules*, 2008, **41**, 1728.
5 K. K. Tenneti, X. Chen, C. Y. Li, X. Wan, X. Fan, Q. F. Zhou, L. Rong and B. S. Hsiao, *Macromolecules*, 2007, **40**, 5095.
6 M. R. Hammond and R. Mezzenga, *Soft Matter*, 2008, **4**, 952.
7 J. Ruokolainen, R. Mäkinen, M. Torkkei, T. Mäkelä, R. Serimaa, G. ten Brinke and O. Ikkala, *Science*, 1998, **280**, 557.
8 I. Vukovic, S. Punzhin, Z. Vukovic, P. Onck, J. T. M. De Hosson, G. ten Brinke and K. Loos, *ACS Nano*, 2011, **5**, 6339.
9 C. Y. Chao, X. Li, C. K. Ober, C. Osuji and E. L. Thomas, *Adv. Funct. Mater.*, 2004, **14**, 364.
10 A. Thünemann, *Prog. Polym. Sci.*, 2002, **27**, 1473.
11 C. F. J. Faul and M. Antonietti, *Adv. Mater.*, 2003, **15**, 673.
12 M. Muthukumar, C. K. Ober and E. L. Thomas, *Science*, 1997, **277**, 1225.
13 N. Merlet-Lacroix, J. Rao, A. Zhang, A. D. Schlüter, S. Bolisetty, J. Ruokolainen and R. Mezzenga, *Macromolecules*, 2010, **43**, 4752.
14 I. W. Hamley, *The Physics of Block Copolymers*, Oxford University Press, Oxford, UK, 1998.
15 J. H. Ryu, N. K. Oh, W. C. Zin and M. Lee, *J. Am. Chem. Soc.*, 2004, **126**, 3551.
16 K. K. Tenneti, X. Chen, C. Y. Li, Y. Tu, X. Wan, Q. F. Zhou, I. Sics and B. S. Hsiao, *J. Am. Chem. Soc.*, 2005, **127**, 15481.
17 K. K. Tenneti, X. Chen, C. Y. Li, X. Wan, X. Fan, Q. F. Zhou, L. Rong and B. S. Hsiao, *Soft Matter*, 2008, **4**, 458.
18 W. Zha, C. D. Han, D. H. Lee, S. H. Han, J. K. Kim, J. H. Kang and C. Park, *Macromolecules*, 2007, **40**, 2109.
19 U. S. Jeng, C. H. Su, C. J. Su, K. F. Liao, W. T. Chuang, Y. H. Lai, J. W. Chang, Y. J. Chen, Y. S. Huang, M. T. Lee, K. L. Yu, J. M. Lin, D. G. Liu, C. F. Chang, C. Y. Liu, C. H. Chang and K. S. Liang, *J. Appl. Crystallogr.*, 2010, **43**, 110.
20 T. J. Hermel, S. F. Hahn, K. A. Chaffin, W. W. Gerberich and F. S. Bates, *Macromolecules*, 2003, **36**, 2190.
21 V. Percec, C. H. Ahn, W. D. Cho, A. M. Jamieson, J. Kim, T. Leman, M. Schmidt, M. Gerle, M. Möller, S. A. Prokhorova, S. S. Sheiko, S. Z. D. Cheng, A. Zhang, G. Uangar and D. J. P. Yeardley, *J. Am. Chem. Soc.*, 1998, **120**, 8619.
22 W. M. Matsen, *Macromolecules*, 1995, **28**, 5765.
23 M. W. Matsen and F. S. Bates, *J. Chem. Phys.*, 1997, **106**, 2436.
24 Y. Y. Huang, H. L. Chen and T. Hashimoto, *Macromolecules*, 2003, **36**, 764.

